

## HIGH FREQUENCY TRANSFORMER LINKED PV INVERTER FOR LIMITING INRUSH CURRENTS AND START-UP OVER VOLTAGES.

**\*GOTTAM SRAVANTHI, \*\*MR.T.VENU GOPAL**

\*PG Scholar, Department of EEE, Vaagdevi College of Engineering( Ugc-Autonomous, Accredited By Nba)

\*\*Associate professor, Department of EEE, Vaagdevi College of Engineering( Ugc-Autonomous, Accredited By Nba)

### ABSTRACT:

We introduce a circuit topology and associated control method suitable for high efficiency DC to AC grid-tied power conversion. This approach is well matched to the requirements of module integrated converters for solar photovoltaic (PV) applications. The topology is based on a series resonant inverter, a high frequency transformer, and a novel half-wave cycloconverter. Zero-voltage switching is used to achieve an average efficiency of 95.9% with promise for exceeding 96.5%. The efficiency is also projected to improve as semiconductor transistor technology develops further. Design and control considerations for the proposed approach are presented, along with experimental results that validate the approach.

### I. INTRODUCTION

#### A. Motivation and Background

The market for roof-top solar panel installations is growing rapidly, and with it grows the demand for inverters to interface with the grid [1]–[3]. Multiple inverter system architectures exist, of which two are the most widely considered. The first approach involves a single grid-tie inverter connected to a series string of PV panels. There are at least two limitations to this approach. Firstly, the maximum power point tracking (MPPT) is performed for the entire series string of panels, which is not optimal given variations among panels and variations in illumination of each panel [2], [4], [5]. Secondly, a permanent defect or even a temporary shade to a single panel in an array, which is controlled by a single inverter, limits the performance of the

entire string [2], [5]. One approach to managing solar arrays is through the use of module integrated converters or microinverters - power converters that are rated for only a few hundreds of watts each, and directly tie an individual panel to the AC grid. Connecting each solar panel via its own micro inverter can improve the overall performance of an installation. One advantage comes from MPPT of each panel's output, which yields greater energy extraction than centralized MPPT of a series-connected string of modules can achieve. Additionally, the performance of the entire installation is no longer limited by failures in individual modules. Although the obvious disadvantage of needing more, smaller inverter modules, each providing much greater voltage transformation, exists for this approach, the trends in residential installations are expected to continue heading in that direction [1], [2],

[4], [6]. In this application, efficiency and compactness are the driving design considerations [6]. There exists an extensive body of work on DC to AC power converters specifically for grid tied PV applications. A thorough overview and a topology classification is provided in [2], [6], [8], [12]. Topologies for different power levels and numbers of phases at the output are also presented in [4], [7], [10], [11], for example. In this paper, we investigate an inverter based on the architecture of Fig. 1, comprising a high-frequency resonant inverter, a high-frequency transformer, and a cycloconverter. This general architecture has long been known (e.g., [7]), but it is perhaps the least explored of known approaches (e.g., see the topology review in [2], [6], [8], [12]). We propose an improved realization of this architecture that enables reduced device losses compared to other realizations along with flexible control, enabling very high efficiencies to be achieved. All devices operate with resistive on-state drops (no diode drops) under zero-voltage switching (ZVS). Moreover, the proposed approach scales favorably with anticipated trends in semiconductor devices.

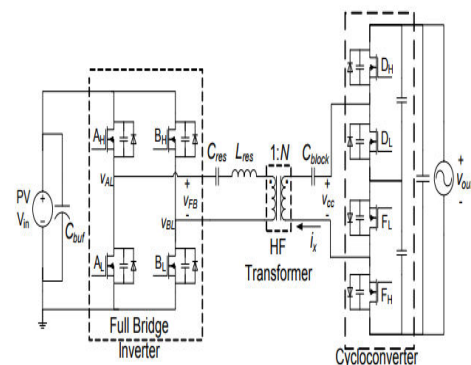
## II. DESIGN

A. Topology Fig. 1 shows the proposed inverter topology. A capacitor bank ( $C_{buf}$ ) placed in parallel with the solar panel provides the necessary twice-line-frequency energy buffering. The size of this capacitance is given by (2), where 'k' is the voltage ripple ratio on the input. For a reasonable ripple ratio of 0.95, the required capacitance is approximately 7.4 mF (as dictated by the lowest nominal input voltage). The buffer comprises electrolytic

capacitors placed in parallel with high-frequency decoupling capacitance to carry the resonant current. A full-bridge series-resonant inverter is operated under variable-frequency phase-shift control, such that each bridge leg is operated at 50% duty ratio under ZVS. For notational convenience the two 'A' MOSFETs form the 'leading' halfbridge leg, with the 'lagging' leg formed by the 'B' MOSFETs. In each half-bridge structure, the subscripts 'H' and 'L' refer to the high and low side device, respectively. The diode and the capacitor across each MOSFET's drain and source represent the parasitic capacitance and body diode of each device. Moreover, additional capacitance may be added across some devices to improve ZVS characteristics (especially in the lagging leg). A high-frequency transformer (turns ratio of 1:N) is combined with the resonant tank components to provide isolation and transformation, yielding a high-frequency quasi-sinusoidal AC current  $i_x$ . A half-wave cycloconverter operates under zero-voltage switching to downconvert the high-frequency AC current, yielding unity-powerfactor output current at line frequency. This cycloconverter, which is new to the authors' knowledge, provides smaller total device drop than conventional bidirectional-blocking-switch topologies, and enables greatly improved layout for high-frequency currents. Operation of the cycloconverter can be summarized as follows: when the line voltage  $v_{out}$  is positive (referenced to the indicated polarity), the bottom two switches of the cycloconverter (FH and FL on Fig. 1) remain on, while the top two switches (DH and DL) form a ZVS half-bridge that modulates the average current (over a switching cycle) delivered into the AC line.

Likewise, for negative output (line) voltages, the top two devices remain on while the bottom two devices modulate the power delivery. Given a low-loss bypass capacitor across each pair of half-bridges in the cycloconverter, the two switches that are on in a given half cycle are effectively in parallel, and so contribute reduced conduction loss compared to a single switch. At any given time, then, cycloconverter conduction loss owing to 1.5 device on-state resistances is obtained, as compared to two on-state resistances for a conventional ‘back-to-back switch’ half-wave cycloconverter. It can also be observed that only one of the two half-bridges modulates at any given time, reducing switching and gating loss in the cycloconverter. Finally, the compactness of the layout of the high-frequency AC paths in the proposed cycloconverter give it substantial practical advantage over conventional ‘back-to-back switch’ cycloconverter topologies. Design decisions embodied in the topology of Fig. 1 focus on achieving high efficiency at small size while meeting the large voltage transformation and isolation requirements. Full-bridge inverter and half-wave cycloconverter topologies are selected because together they reduce the required transformer turns ratio (e.g., as compared to using a half-bridge inverter or a full-wave cycloconverter), thus improving achievable efficiency. Likewise, by eliminating diode drops from main operation of the converter, and by operating all of the (resistive on-state) devices under zero-voltage switching as described below, one can achieve low loss by scaling device areas up beyond that which is optimum for hard-switched topologies. Moreover, given an absence of diode drops in the main conversion path, the efficiency

achievable with this topology is expected to improve as the characteristics of resistive drop devices continue to improve. Finally, we are able to absorb transformer leakage as part of the resonant inductor, facilitating at least partial component integration. Note that the capacitor ( $C_{block}$ ) placed on the secondary side of the transformer is not a resonant element, but merely ensures that no DC is present that can possibly saturate the transformer. Its value has to be large enough not to significantly affect the total effective capacitance of the main circuit loop. The entire resonant tank may be placed on either the primary or the secondary side of the transformer as long as the inductance and capacitance are scaled appropriately. The DC blocking capacitor is placed on the side opposite that of the resonant capacitor. The benefit of placing the resonant components on the primary side arises from the presence of an effective parasitic capacitance across the (high-voltage) transformer secondary. When there are no resonant components on the secondary, this capacitance is absorbed into the overall capacitance across the cycloconverter. This reduces the ringing, which could be present in the resonant current waveforms due to the charging and discharging of the parasitic capacitance.



## GRID CONNECTED PV SYSTEMS

This chapter highlights the advantages of transformerless PV inverters compared to those with galvanic isolation. Furthermore, a summary of several transformerless PV inverter topologies is presented, followed by discussions about the parasitic capacitance of the PV array, emphasizing the safety issues regarding ground leakage currents due to varying voltages imposed over this capacitance. PV systems connected to the low voltage grid have an important role in distributed generation systems. In order to keep up with the current trends regarding the increase in PV installations, PV inverters should have the following characteristics:

- Low cost
- Small weight and size, due to residential installations
- High reliability to match with that of PV panels
- High efficiency
- Be safe for human interaction

During the last decade PV inverter technologies have evolved a lot. As shown in Figure, inverter prices have dropped around 50% during the last two decades and efficiency and reliability have increased considerably. Depending of the power rating of the inverter, the price of inverters below 10 kW varies between 0.2 and 1.2 euro/kW excluding VAT. All this development and improvement happened especially in Europe, USA and Japan. Here one can find many small-scale, building integrated systems that are connected to the grid. In order to decrease the cost-to-efficiency ratio of PV systems, new inverter designs have been developed.

A general classification of grid connected PV inverters is as follows.

- Central inverters
- String inverters
- Module integrated inverters
- Multi-string inverters

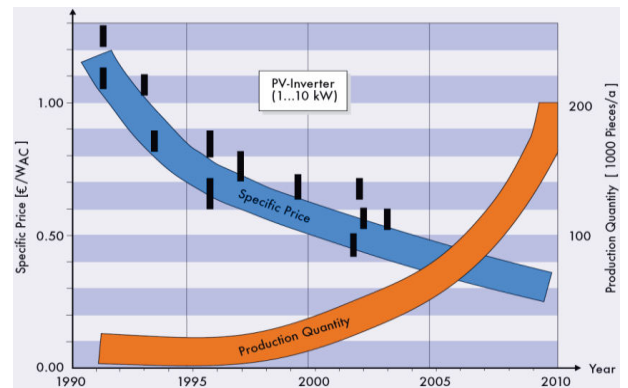


Figure 2: Development and prognoses of specific cost and production quantity for a PV inverter of nominal power between 1 and 10kW during the last two decades.

## CONVENTIONAL PRECHARGE OF THE SECONDARY-SIDELINK VOLTAGE

It is assumed that the input dc bus  $V_{dc}$  is precharged. For the full bridge topology with lossless snubber in the snubberswitch  $S$  is assumed to be ON so that the snubber capacitor can be precharged to a dc voltage. Conventional approaches reported in the literature for precharging the link voltage [11]–[13] are analyzed in the following sections and the related issues are detailed. The start-up methods in the literature having additional start-up circuitry [16]–[18] are not evaluated as these methods increase the system cost and complexity. It must be noted that the start-up method proposed in this paper does not require any additional power or control circuit hardware.

## A. Square-Wave Modulation With Diode Rectifier

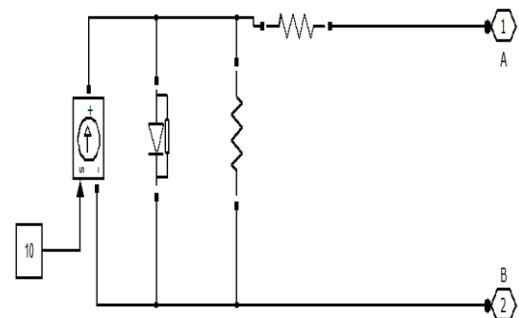
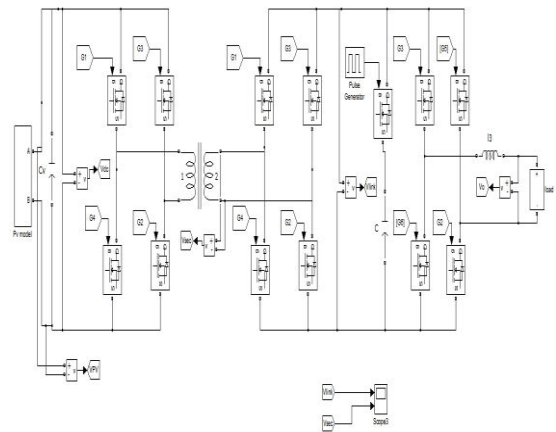
In this method, the HF inverter devices are switched in square wave mode. In other words, the transformer primary voltage is a square wave. The HF inverter switches have a duty ratio  $D = 0.5$ . The HF rectifier IGBTs are all OFF. Hence, the rectification is done by the diodes only. This is a simplest start-up method that can be considered for HF transformer link inverters. However, this method has significant limitations which are explained below.

**1) Over-voltage problem:** The start-up equivalent circuit for this case is shown in Fig. 4. The snubber switch is ON hence the capacitor  $C_s$  is directly connected to dc link as in case of DAB

fed inverter. A bleeder resistor  $R_{bl}$  is shown across  $C_s$ . This is normally used to fasten the discharge of  $C_s$  when the inverter is turned OFF. The primary voltage is replaced by a square wave voltage source. The output inverter is inactive as all the switches are OFF and hence it is not shown in the equivalent circuit. The rectifier IGBTs are switched OFF as only the diodes are used for rectification. Hence, the IGBTs are shown in light shade. With an ideal transformer, the rectified voltage will be purely dc with amplitude of the primary voltage. However, practically the HF transformer has a stray capacitance appearing in its equivalent circuit [22]. This leads to a resonance when the input voltage has step-change. The parameters of the HF transformer equivalent circuit model are determined using a network analyzer. The HF transformer is connected in open-circuit and short-circuit configurations to the network analyzer to determine the parameters of the equivalent

circuit. A simplified procedure is adopted to determine these parameters. Due to the resonance, the reflected secondary voltage goes beyond the primary voltage and reverse biases the diodes in HF rectifier. This results in the link capacitance charging to a higher voltage than the amplitude of primary voltage. As PV inverter topologies have to operate between open-circuit voltage to maximum power point (MPP) voltage, the start-up overvoltage can exceed the voltage rating or can considerably reduce the safe operating margin of semiconductor devices.

## SIMULATION RESULTS:



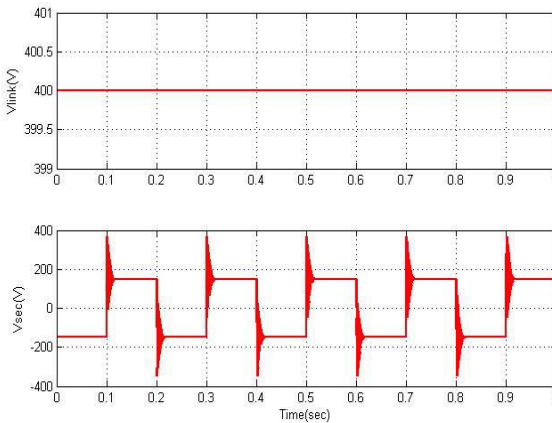
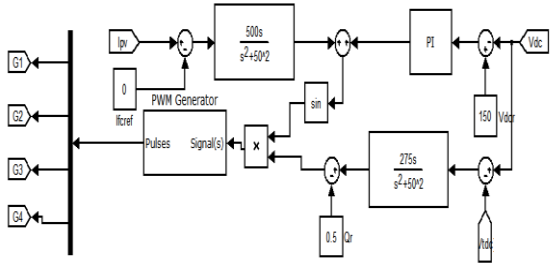


Fig. 6: Simulation results of Precharge of the link voltage  $V_{link}$  with  $D = 0.5$  and passive rectifier.  $V_{in} = 30$

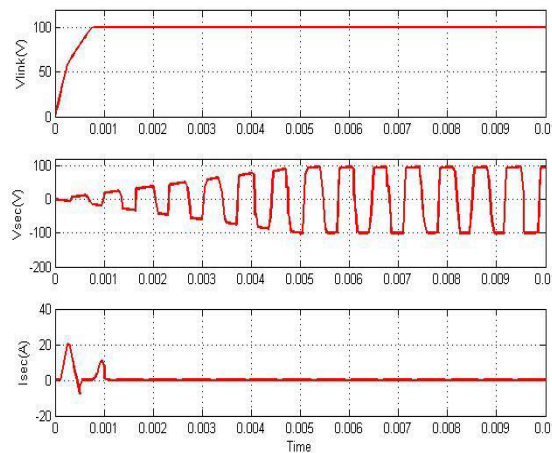


Fig. 8. Simulink results Inrush secondary current and building up of secondary voltage and link voltage for  $D = 0.5$  and input voltage  $V_{in} = 10V$ .

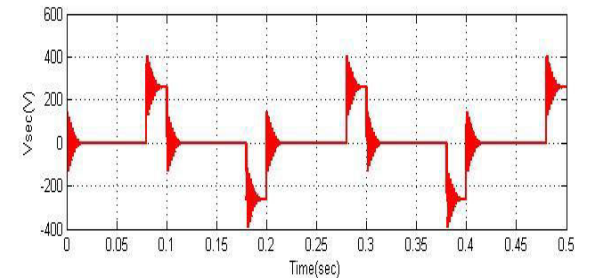
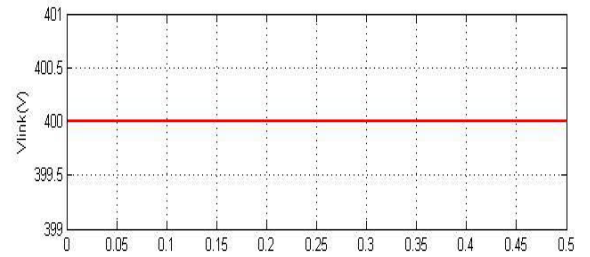


Fig. 10. Simulation results Precharge of the link voltage  $V_{link}$  with  $D = 0.08$  and passive rectifier.

$V_{in} = 30 V$ .

## CONCLUSION:

A hybrid ac/dc microgrid is proposed and comprehensively studied in this paper. The models and coordination control schemes are proposed for the all the converters to maintain stable system operation under various load and resource conditions. The coordinated control strategies are verified by MATLAB/Simulink. Various control methods have been incorporated to harness the maximum power from dc and ac sources and to coordinate the power exchange between dc and ac grid. Different resource conditions and load capacities are tested to validate the control methods. The simulation results show that the hybrid grid can operate stably in the grid-tied or isolated mode. Stable ac and dc bus voltage can be guaranteed when the operating conditions or load capacities change in the

twomodes. The power is smoothly transferred when load condition changes. Although the hybrid grid can reduce the processes of dc/ac and ac/dc conversions in an individual ac or dc grid, there are many practical problems for implementing the hybrid grid based on the current ac dominated infrastructure. The total system efficiency depends on the reduction of conversion losses and the increase for an extra dc link. It is also difficult for companies to redesign their home and office products without the embedded ac/dc rectifiers although it is theoretically possible. Therefore, the hybrid grids may be implemented when some small customers want to install their own PV systems on the roofs and are willing to use LED lighting systems and EV charging systems. The hybrid grid may also be feasible for some small isolated industrial plants with both PV system and wind turbine generator as the major power supply.

## REFERENCES

- [1] R. H. Lasseter, "MicroGrids," in Proc. *IEEE Power Eng. Soc. Winter Meet.*, Jan. 2002, vol. 1, pp. 305–308.
- [2] Y. Zoka, H. Sasaki, N. Yorino, K. Kawahara, and C. C. Liu, "An interaction problem of distributed generators installed in a Micro Grid," in Proc. *IEEE Elect. Utility Deregulation, Restructuring. Power Technol.*, Apr. 2004, vol. 2, pp. 795–799.
- [3] R. H. Lasseter and P. Paigi, "Micro grid: A conceptual solution," in Proc. *IEEE 35th PESC*, Jun. 2004, vol. 6, pp. 4285–4290.
- [4] C. K. Sao and P. W. Lehn, "Control and power management of converter fed Micro Grids," *IEEE Trans. Power Syst.*, vol. 23, no. 3, pp. 1088–1098, Aug. 2008.
- [5] T. Logenthiran, D. Srinivasan, and D. Wong, "Multi-agent coordination for DER in Micro Grid," in Proc. *IEEE Int. Conf. Sustainable Energy Technol.*, Nov. 2008, pp. 77–82.
- [6] M. E. Baran and N. R. Mahajan, "DC distribution for industrial systems: Opportunities and challenges," *IEEE Trans. Ind. Appl.*, vol. 39, no. 6, pp. 1596–1601, Nov. 2003.
- [7] Y. Ito, Z. Yang, and H. Akagi, "DC micro-grid based distribution power generation system," in Proc. *IEEE Int. Power Electron. Motion Control Conf.*, Aug. 2004, vol. 3, pp. 1740–1745.
- [8] A. Sannino, G. Postiglione, and M. H. J. Bollen, "Feasibility of a DC network for commercial facilities," *IEEE Trans. Ind. Appl.*, vol. 39, no. 5, pp. 1409–1507, Sep. 2003.
- [9] D. J. Hammerstrom, "AC versus DC distribution systems-did we get it right?," in Proc. *IEEE Power Eng. Soc. Gen. Meet.*, Jun. 2007, pp. 1–5.
- [10] D. Salomonsson and A. Sannino, "Low-voltage DC distribution system for commercial power systems with sensitive electronic loads," *IEEE Trans. Power Del.*, vol. 22, no. 3, pp. 1620–1627, Jul. 2007.
- [11] M. E. Ropp and S. Gonzalez, "Development of a MATLAB/Simulink model of a single-phase grid-connected photovoltaic system," *IEEE Trans. Energy Conv.*, vol. 24, no. 1, pp. 195–202, Mar. 2009.
- [12] K. H. Chao, C. J. Li, and S. H. Ho, "Modeling and fault simulation of photovoltaic generation systems using circuit-based model,"



in Proc.*IEEE* Int. Conf. Sustainable Energy Technol., Nov. 2008, pp. 290–294.

[13] O. Tremblay, L. A. Dessaint, and A. I. Dekkiche, “A generic battery model for the dynamic simulation of hybrid electric vehicles,” in Proc.*IEEE* Veh. Power Propulsion Conf. (VPPC 2007), pp. 284–289.

[14] D. W. Zhi and L. Xu, “Direct power control of DFIG with constant switching

frequency and improved transient performance,” *IEEE* Trans. Energy Conv., vol. 22, no. 1, pp. 110–118, Mar. 2007.

[15] L. Bo and M. Shahidehpour, “Short-term scheduling of battery in a grid-connected PV/battery system,” *IEEE* Trans. Power Syst., vol. 20, no. 2, pp. 1053–1061, May 2005.